Diffusion-weighted MR Imaging of Female Pelvic Tumors: A Pictorial Review[1]

Charlotte S. Whittaker, MRCP, FRCR • Andy Coady, MRCPath • Linda Culver, DCR(R) • Gordon Rustin, MD, FRCP • Malcolm Padwick, MD, FRCOG • Anwar R. Padhani, FRCP, FRCR

TEACHING POINTS
See last page

Functional imaging is becoming increasingly important in the evaluation of cancer patients because of the limitations of morphologic imaging, particularly in the assessment of response to therapy. Diffusion-weighted magnetic resonance (MR) imaging has been established as a useful functional imaging tool in neurologic applications for a number of years, but recent technical advances now allow its use in abdominal and pelvic applications. Diffusion-weighted MR imaging studies of female pelvic tumors have shown reduced apparent diffusion coefficient (ADC) values within cervical and endometrial tumors. In addition, this unique noninvasive modality has demonstrated the capacity to help discriminate between benign and malignant uterine lesions and to help assess the extent of peritoneal spread from gynecologic malignancies. Potential pitfalls can be avoided by reviewing diffusion-weighted MR imaging findings in conjunction with anatomic imaging findings. Increasing familiarity with ADC calculation and manipulation software will allow radiologists to provide new information for the care of patients with known or suspected gynecologic malignancies.

Abbreviation: ADC = apparent diffusion coefficient

RadioGraphics 2009; 29:759–778 • **Published online** 10.1148/rg.293085130 • **Content Codes:** GU MR OB OI

[1]From the Paul Strickland Scanner Centre, Mount Vernon Cancer Centre, Rickmansworth Rd, Northwood, Middlesex HA6 2RN, England. Presented as an education exhibit at the 2007 RSNA Annual Meeting. Received May 8, 2008; revision requested June 24 and received August 23; accepted September 19. C.S.W. is the spouse of an employee of Amgen; A.R.P. is an associate medical director with Synarc; all other authors have no financial relationships to disclose. **Address correspondence to** C.S.W. (e-mail: *c_whittaker1@yahoo.co.uk*).

See the commentary by Jha following this article.

Table 1
Protocol for Diffusion-weighted MR Imaging of the Pelvis

Parameter	Purpose of Acquisition	
	ADC Calculation	Creation of Fusion Images
Repetition time (msec)	3500	3500
Echo time (msec)	98	92
Bandwidth (Hz/pixel)	1010	1000
b values (sec/mm^2)	0, 50, 100, 250, 500, 750	900, 1100, 1300
Field of view (cm)	22.4 or 26	22.4 or 26
Image matrix*	120 × 190	83 × 156
Acceleration factor	2	2
Number of signals acquired	6	6
Acquisition time (min)	6.48	4.7

Note.—This protocol was developed for studies conducted with a 1.5-T imager and the following additional parameters: single-shot, fat-suppressed T2-weighted echoplanar imaging with diffusion weighting and parallel imaging acceleration; non-breath-hold technique; 6-mm section thickness; and 90° flip angle.
*Increase matrix size if needed.

Introduction

Diffusion-weighted magnetic resonance (MR) imaging is a functional imaging technique whose contrast derives from the random motion of water molecules within tissues. Although its use in intracranial imaging has been established for a number of years (1), problems with motion and susceptibility artifacts have limited its application in abdominal and pelvic imaging. However, the development of new imaging techniques, particularly novel methods of data acquisition and parallel imaging, has allowed much faster data acquisition with fewer artifacts, resulting in significant improvement in image quality in body applications. Because image contrast is derived from inherent differences in the restriction of the movement of water molecules, no exogenous contrast medium administration is required, so that diffusion-weighted sequences can now be included in routine patient assessment.

When diffusion-weighted MR imaging is used in gynecologic applications, cervical cancers have been shown to have significantly lower apparent diffusion coefficient (ADC) values compared with normal cervical tissue (2,3). Similar findings have been noted in endometrial cancers, with a tendency toward lower ADC values in higher-grade lesions (4,5). In addition, diffusion-weighted MR imaging shows promise as a biomarker for treatment response, with increasing ADC values noted in cervical carcinomas responding to radiation therapy (2). Diffusion-weighted MR imaging also shows promise in discriminating between benign and malignant lesions within the myometrium and endometrial cavity (6,7) and in detecting peritoneal dissemination of gynecologic tumors (8). In this article, we review the means of acquiring diffusion-weighted MR images, discuss and illustrate the clinical applications of this modality in women with gynecologic malignancies, provide image interpretation guidelines, and discuss potential pitfalls.

Measurement and Analysis with Diffusion-weighted MR Imaging

Use of MR imaging to demonstrate the contribution of water diffusion to image contrast was first described by Stejskal and Tanner (9), who applied symmetric pairs of equally weighted diffusion sensitizing gradients about the 180° refocusing pulse of a spin-echo T2-weighted sequence. Static water molecules develop additional phase incoherencies from the application of the first diffusion gradient, but these incoherencies are eliminated by the application of the second gradient, resulting in no additional net loss of signal (aside from normal T2 decay). However, mobile water is not completely rephased by the second gradient owing to movement to a different microenvironment during the application of the first gradient, so that a subsequent reduction in signal intensity is observed. Altering the gradient amplitude,

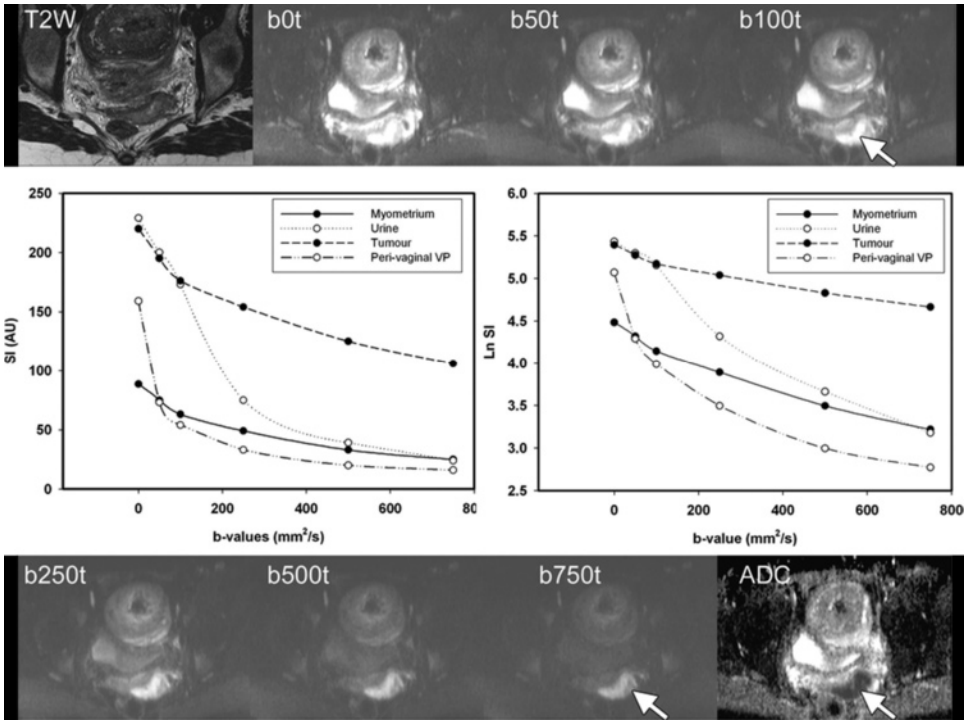

Figure 1. Calculation of ADC from signal intensity data obtained in a 26-year-old woman who had given birth 10 days earlier. T2-weighted MR image, *b*-value images (*b* = 0, 50, 100, 250, 500, and 750 sec/mm^2), and corresponding ADC map show a poorly differentiated vaginal squamous cell carcinoma (arrow). Graphs illustrate how ADC values were calculated in terms of the natural logarithm *(Ln)* of signal intensity *(SI)* (y axis) versus trace *b* values (*b* = 0–750 sec/mm^2) (x axis). *AU* = arbitrary units. Note the biexponential behavior of the perivaginal venous plexus. Interestingly, urine does not appear to demonstrate monoexponential decay. Calculated ADC values were as follows: urine = 3044×10^{-6} mm^2/sec, perivaginal venous plexus = 2500×10^{-6} mm^2/sec, myometrium = $15{,}474 \times 10^{-6}$ mm^2/sec, and tumor = 852×10^{-6} mm^2/sec.

duration, and time interval (*b* value, measured in seconds per square millimeter) between paired diffusion gradients will alter sensitivity to the degree of water motion (1).

Tissues containing water that is moving the most freely (eg, within blood vessels, ducts, or the bladder) will demonstrate greater signal losses after the application of the smallest diffusion gradients (<100 sec/mm^2). Signal losses caused by water motion in the extracellular space of tumors occur at higher *b* values because water motion is modified by interactions with hydrophobic cell membranes and macromolecules (increased extracellular space tortuosity) (10). In solid tumors of high cellularity, there are additional significant reductions in extracellular space, resulting in further restrictions to free water movement.

In clinical practice, diffusion-weighted MR imaging is usually performed at two or more *b* values, which always include one or more low *b* values (0 or 50 sec/mm^2) and a very high *b* value (usually ~1000 sec/mm^2). In our practice, we perform two separate data acquisitions for two distinct purposes (Table 1). In the first acquisition, we acquire images at six *b* values to calculate an accurate ADC value. In the second acquisition, we acquire images at much greater *b* values to completely eliminate all background signal and reduce T2 shine-through (defined later). Details concerning fat-suppression schemes, different ways of applying diffusion gradients to minimize artifacts, sequence optimization, and strategies for maximizing signal-to-noise ratio can be found in an excellent recent article by Koh et al (11).

The ADC value (measured in square millimeters per second) is usually calculated by the slope of the line of the natural logarithm of signal intensity (y axis) versus *b* values (x axis) (Fig 1).

Table 2
Scheme for the Interpretation of Diffusion-weighted MR Imaging Findings

Signal Intensity on T2-weighted Images	Signal Intensity on High *b*-Value Source Images*	Values on ADC Maps	Interpretation of Findings
Isointensity, hyperintensity	Hyperintensity	Decreased	Generally, high-cellularity tumor; rarely, coagulative necrosis, highly viscous fluid, or abscess
Hyperintensity	Hyperintensity	Increased	T2 shine-through; often, proteinaceous fluid
Hypointensity, isointensity	Hypointensity	Decreased	Fibrous tissue with low water content with or without viable tumor cells
Hyperintensity	Hypointensity	Increased	Fluid, liquefactive necrosis, lower cellularity, gland formation

*b > 800 sec/mm^2.

In effect, this yields a monoexponential "fit" for the raw signal intensity data, although in practice, water diffusion in tissues is biexponential, the first exponent representing water movement in vessels and the second representing extravascular water movement. ADC maps are usually displayed parametrically as gray-scale images. Areas of restricted diffusion have lower ADC values and therefore are a darker shade of gray on ADC maps, whereas areas of freely moving water (eg, within cysts or the bladder) will be a lighter shade of gray. The opposite is true with the source high *b*-value images (b = 800–1000 sec/mm^2), on which areas of restricted diffusion mostly appear bright. It is important to remember that ADC maps and high *b*-value images should never be interpreted in isolation, but should be interpreted together with anatomic images according to the scheme outlined in Table 2 so as to avoid the pitfalls that will be discussed shortly. Figure 2 shows a typical series of images from an examination of a normal female pelvis.

Teaching Point

There are a number of ways to display very high *b*-value images (on which fat and background suppression is maximal). Because the signal is essentially nonquantitative, an inverted gray scale or arbitrary color scales (false color map) are often used. Data sets can be visualized with use of multiplanar reconstruction and maximum intensity projection and are amenable to volume rendering. Such data are also amenable to fusion imaging to allow coregistration to anatomic images. Fusion imaging is performed in three steps: *(a)* superimposition (data sets do not need to be in the same plane or to have identical fields of view or matrix sizes); *(b)* alignment with sophisticated computer algorithms, usually on the basis of anatomic landmarks; and *(c)* blending of gray-scale anatomic and pseudocolor *b*-value images, with the ability to adjust the balance between the two superimposed data sets. It is important to remember that internal organ motion in the time interval between data acquisitions may necessitate additional manual or automated registrations.

Teaching Point

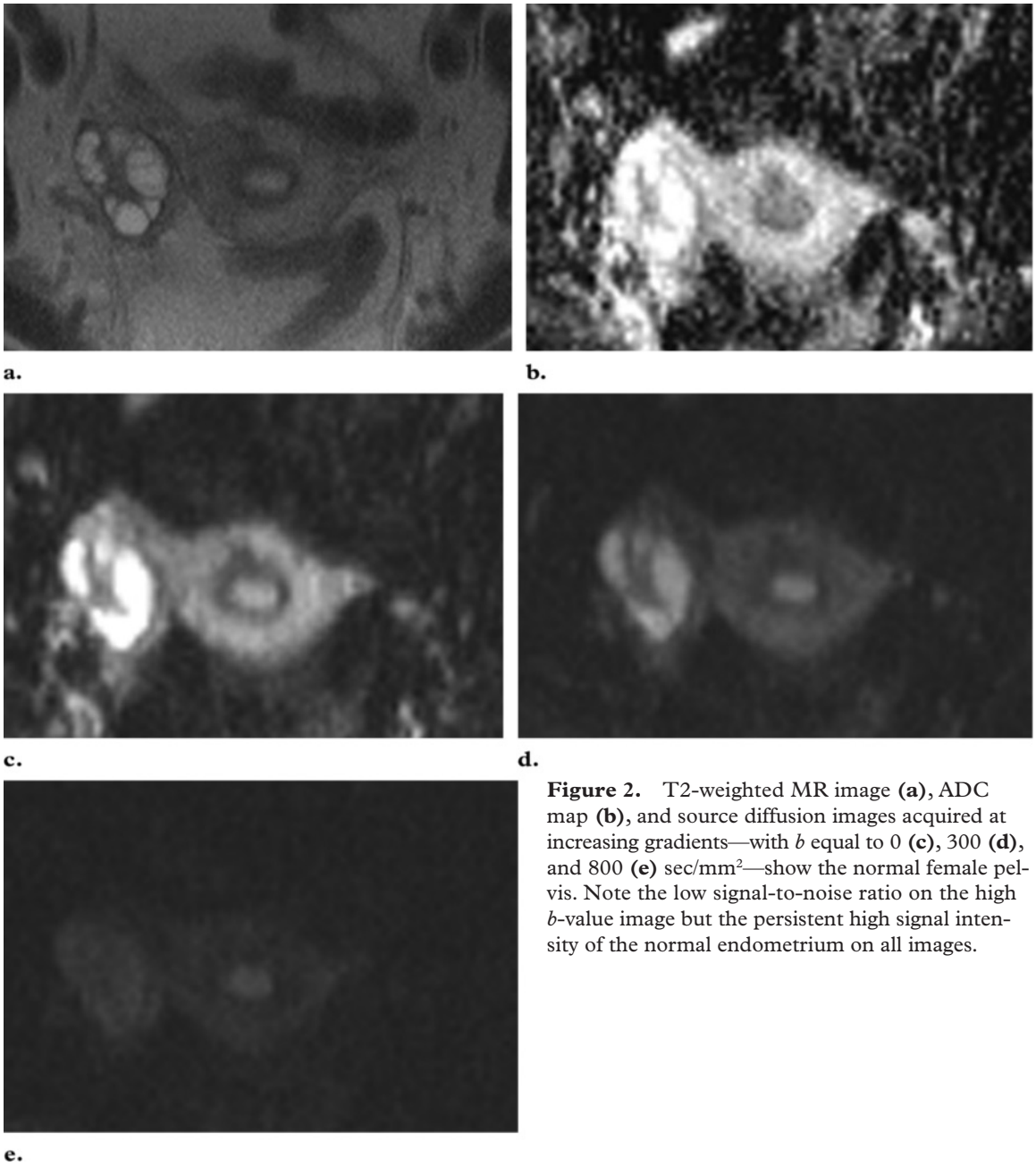

Figure 2. T2-weighted MR image **(a)**, ADC map **(b)**, and source diffusion images acquired at increasing gradients—with *b* equal to 0 **(c)**, 300 **(d)**, and 800 **(e)** sec/mm^2—show the normal female pelvis. Note the low signal-to-noise ratio on the high *b*-value image but the persistent high signal intensity of the normal endometrium on all images.

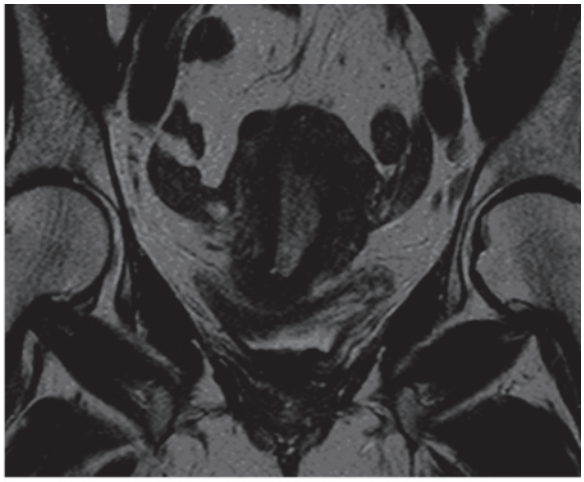

a.

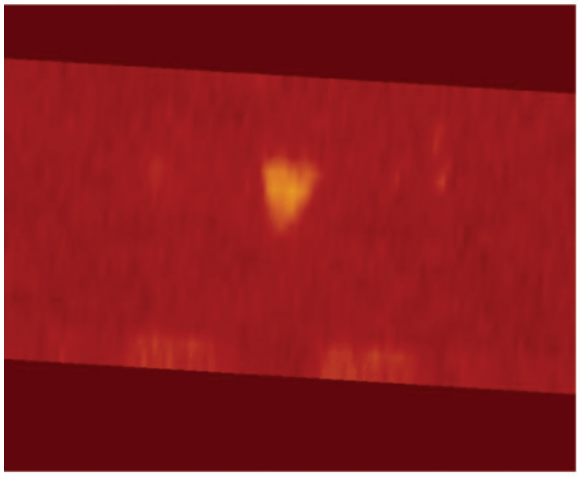

b.

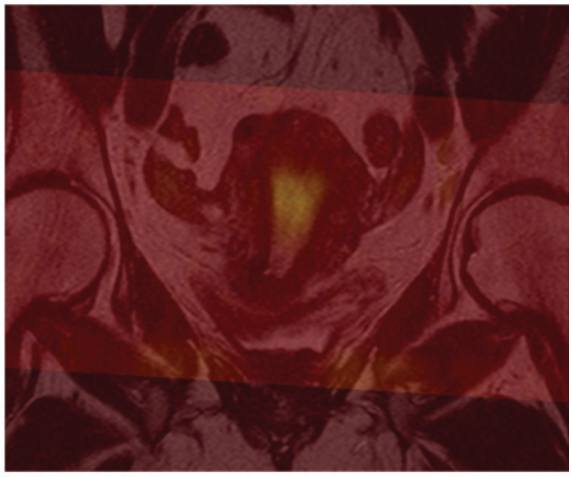

c.

Figure 3. T1a endometrial carcinoma in a 62-year-old woman. **(a, b)** Coronal T2-weighted MR image **(a)** and false color map derived from a high *b*-value image (b = 800 sec/mm^2) **(b)** show a T1a endometrial carcinoma. **(c)** Fused image (**b** superimposed on **a**) clearly shows the absence of myometrial invasion.

Clinical Applications of Diffusion-weighted MR Imaging of Gynecologic Tumors

Determining Depth of Invasion

Because high *b*-value images show tumors of high cellularity to be very bright, they can be fused with anatomic T2-weighted images to improve visualization of the depth of tumor invasion, particularly invasion of the myometrium by endometrial cancer. Contrast material–enhanced fat-suppressed images have traditionally been used because the junctional zone required for determining depth of invasion with T2-weighted sequences may not always be readily appreciated, particularly in postmenopausal patients or in patients with myometrial thinning. Dynamic sequences are helpful for visualizing depth of invasion because the majority of tumors are hypovascular relative to the vascular myometrium. However, a significant number of tumors are either iso- or hypervascular relative to the myometrium. Because diffusion-weighted imaging is essentially independent of differences in vascularity, it is useful for determining T stage

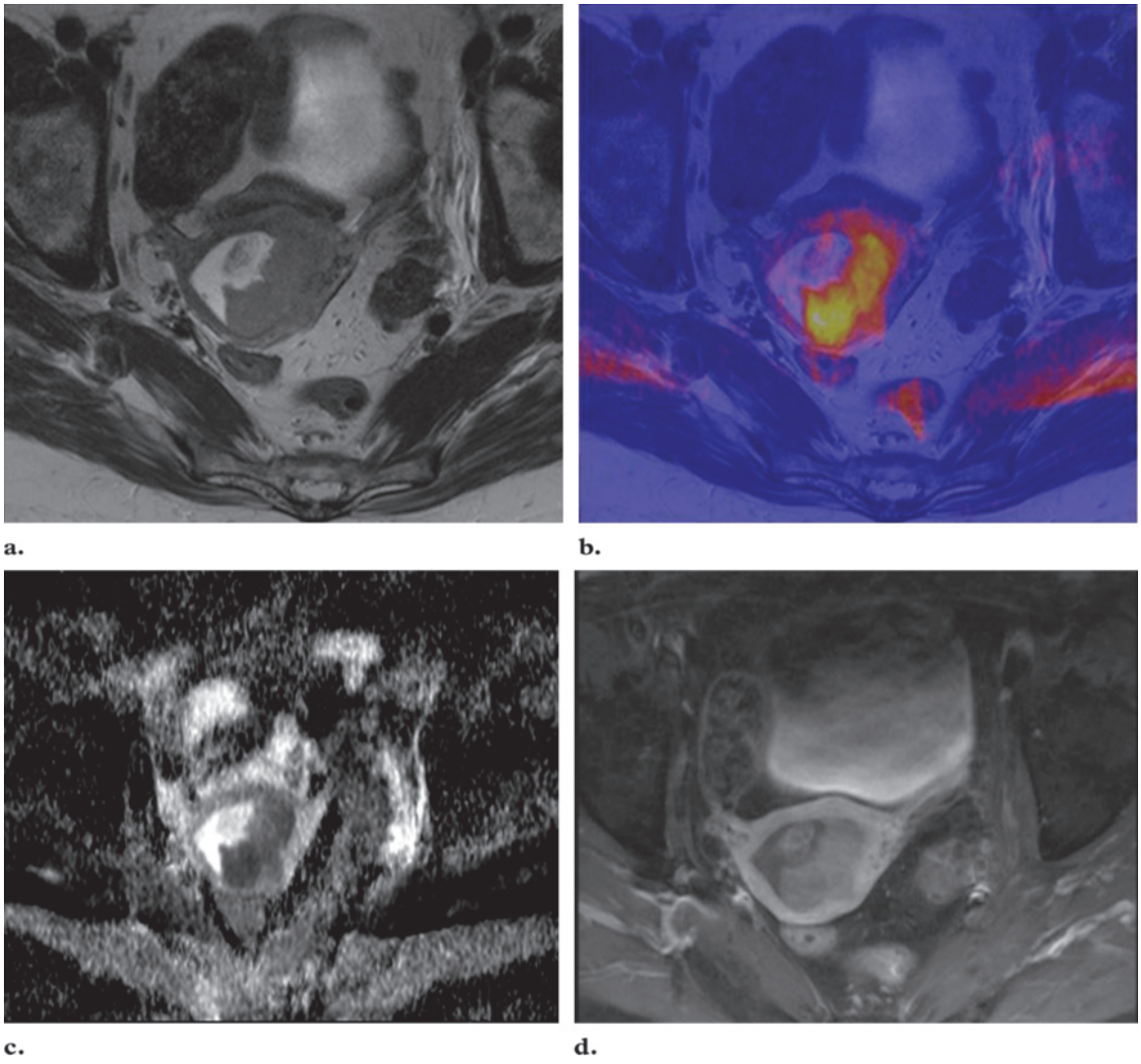

Figure 4. T1c endometrial carcinoma in a 74-year-old woman who underwent a staging examination. Axial T2-weighted MR image **(a)**, fused high *b*-value (b = 1000 sec/mm^2)–axial T2-weighted MR image **(b)**, ADC map **(c)**, and gadolinium-enhanced fat-saturated T1-weighted MR image **(d)** show deep myometrial invasion but no serosal involvement. The mass is hypovascular and shows significant restriction to water diffusion, findings that indicate that the mass is highly cellular. The mass was confirmed to be a high-grade papillary serous carcinoma at histologic analysis.

in such cases. Shen et al (12) also found that diffusion-weighted imaging depicted tumor foci that were not appreciated with T2-weighted or dynamic sequences, such as elsewhere in the uterus or in peritoneal spread. In addition, it may not always be possible to perform contrast-enhanced imaging due to factors such as renal failure.

Figures 3 and 4 illustrate typical appearances of endometrial carcinoma. Note the differing appearances of the superficial tumor in Figure 3 and the mass in Figure 4, which demonstrates deeper myometrial invasion.

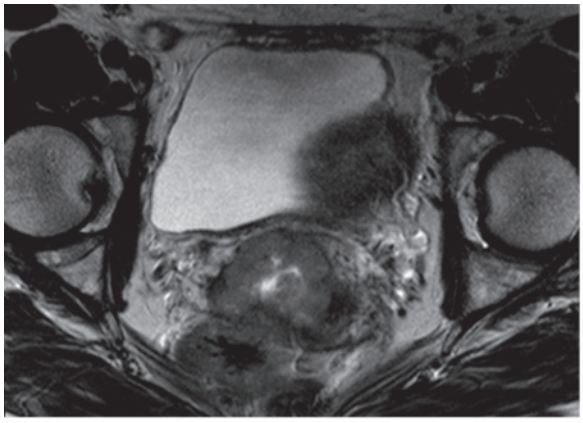

5a.

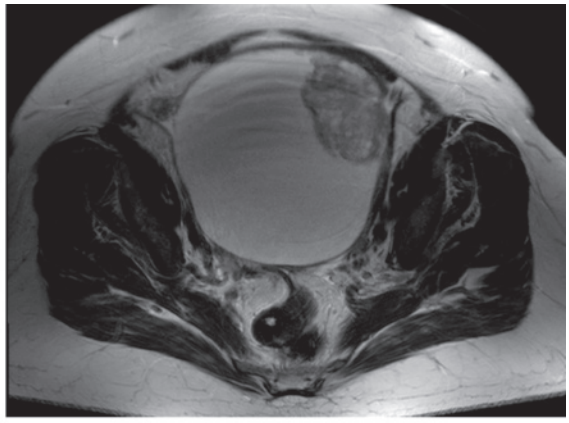

6a.

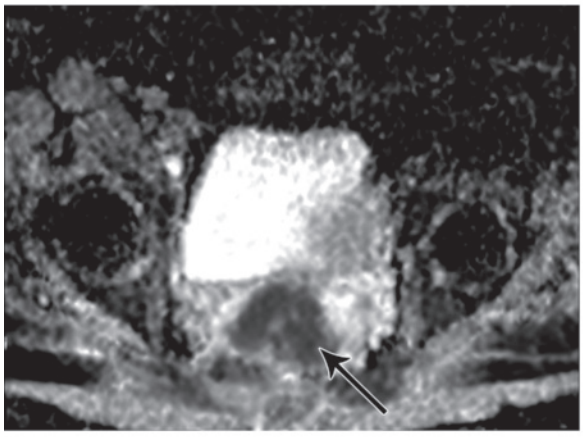

5b.

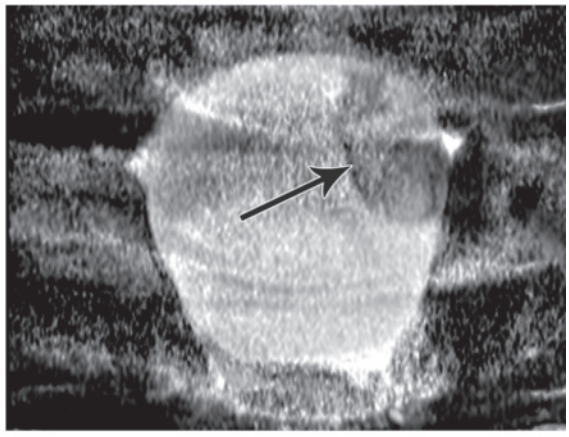

6b.

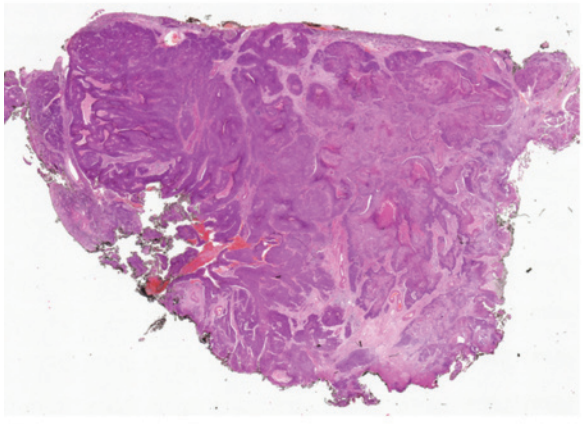

5c.

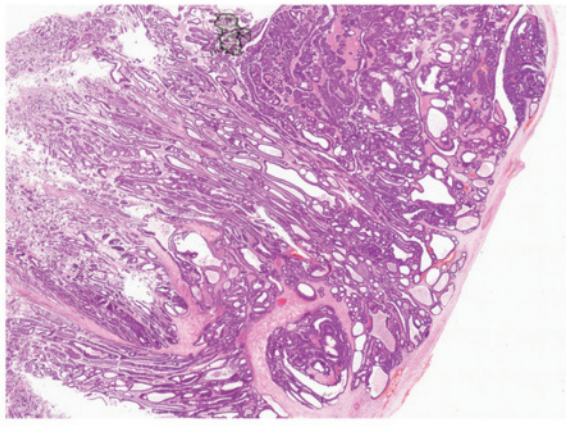

6c.

Figures 5, 6. **(5)** Extensive poorly differentiated squamous carcinoma of the cervix in a 48-year-old woman. **(a)** Axial T2-weighted MR image shows a bulky tumor with parametrial extension. **(b)** ADC map shows a very low ADC value within the tumor (arrow), a finding that is consistent with a hypercellular lesion. **(c)** Photomicrograph (hematoxylin-eosin stain) of a cone biopsy specimen shows vascular invasion of the entire specimen. **(6)** Endometrial carcinoma in a 68-year-old woman. **(a)** T2-weighted MR image from the staging examination shows a complex cystic mass arising from the left ovary. **(b)** On the corresponding ADC map, restriction is visible only at the edge of the solid component (arrow). **(c)** Photomicrograph (hematoxylin-eosin stain) shows a well-differentiated endometrioid carcinoma. Glandular elements are also visible.

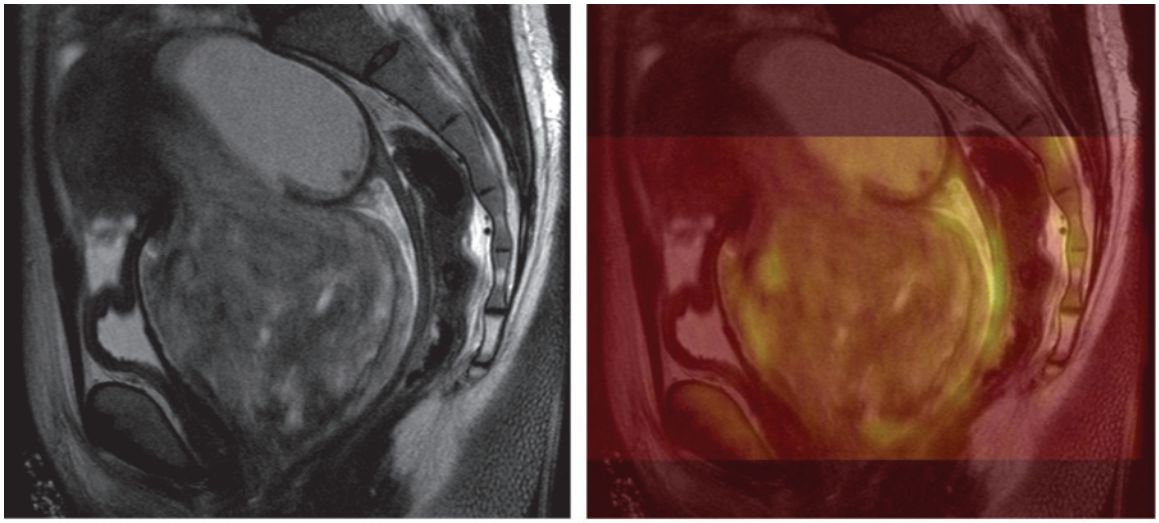

a. b.

Figure 7. Prolapsed submucosal leiomyoma in a 37-year-old woman who presented with a vaginal mass. **(a)** Sagittal T2-weighted MR image shows a large, pedunculated lesion arising from the anterior part of the myometrium and prolapsing through the external os of the cervix. **(b)** Fused image (high *b*-value image [*b* = 800 sec/mm^2] superimposed on **a**) shows no significant restriction. No suspicious findings were noted at histologic analysis.

Lesion Characterization

With increasing tumor cellularity and architectural distortion, there is a reduction in extracellular space, which also becomes increasingly tortuous. These changes are reflected by a reduced ADC value. High-grade adenocarcinomas typically have high cellular density and so would be expected to have lower ADC values. A trend toward lower ADC values in higher-grade endometrial cancers was noted by Tamai et al (4), although this trend did not achieve statistical significance in their study. Figure 5 shows a cervical carcinoma extending through the cervical stroma into the parametrium and upper third of the vagina. A markedly low ADC value (930×10^{-6} mm^2/sec) was measured within the tumor.

Teaching Point

Unfortunately, there is no definite ADC cutoff value that is predictive of the presence of malignancy in the pelvis, partly because the calculated ADC value is dependent on the range of *b* values used for calculations. Low ADC values can be seen in some normal tissues (eg, peripheral nerves, normal lymph nodes, and, occasionally, normal endometrium and bowel) as well as in areas of fibrosis. It should also be noted that well-differentiated tumors and necrotic poorly differentiated tumors can both have increased ADC values (10). Figure 6 illustrates a well-differentiated endometrioid carcinoma of the ovary with cystic and solid components. It should be noted that cellularity is only one feature used to determine tumor grade, and that other indicators such as nuclear atypia are also important but are not assessed with diffusion-weighted MR imaging. Necrosis (an indicator of poor differentiation) is a further confounding factor because it increases ADC values.

The possibility of discriminating between benign and malignant lesions of the uterus with diffusion-weighted MR imaging has been investigated (6,7). Tamai et al (6) found that the mean ADC value of uterine sarcomas was significantly lower than that of normal myometrium and of leiomyomas. A variety of lesions of the endometrial cavity were evaluated by Fujii et al (7), who found that malignant lesions such as endometrial carcinoma and carcinosarcoma had lower ADC values than did benign lesions, including submucosal leiomyomas (Fig 7) and endometrial polyps.

Node Assessment

The use of node size alone to determine the presence of metastatic lymphadenopathy has been shown to be a poor discriminator in pelvic imaging (13). Several investigators have studied

the use of diffusion-weighted MR imaging in the neck to evaluate visible lymph nodes and have found that the ADC value is significantly lower in lymphomatous nodes than in metastatic nodes (14,15). This observation is likely related to the hypercellular nature of the lymphomatous nodes and to the presence of necrosis noted in squamous cell head and neck carcinomas. To our knowledge, firm data on nodal diffusion-weighted MR imaging of pelvic cancers have not appeared in the peer-reviewed literature, and in our experience with female pelvic cancers, both benign and metastatic lymph nodes appear bright on high *b*-value images, with corresponding low ADC values (Figs 8, 9). Our criterion for identifying a suspect lymph node at diffusion-weighted MR imaging takes into account its signal intensity on very high *b*-value images (b >1000 sec/mm^2) relative to that of nodes that we "know" are benign (eg, groin nodes in patients with endometrial or cervical cancer). However, the presence of necrosis within involved nodes is a potential pitfall and should be considered. Another approach is to compare the signal intensity of a lymph node with that of the primary tumor. It should be noted in passing that high *b*-value images can be used for node mapping and can help increase the visibility of pelvic nodes, which can be limited in women with ascites or a paucity of pelvic fat.

Assessment of Treatment Response

The measurement of change in tumor size is the standard method of evaluating treatment response in clinical practice but has a number of shortcomings (16). Because many therapies induce cellular lysis, it is expected that there will be an increase in water diffusion distances within tumors. A number of studies have demonstrated increases in ADC value following successful therapy (17–19), although there is a paucity of data regarding female pelvic tumors. Naganawa et al (2) found significant increases in lesion ADC values in patients with cervical cancer who were treated with combined chemotherapy–radiation therapy. The success of therapy can be assessed both quantitatively with ADC measurements and qualitatively by inspecting signal intensity on high *b*-value images.

Teaching Point

Rapid increases in ADC values are seen following chemotherapy, resulting in cellular apoptosis, whereas changes in perfusion as depicted with dynamic sequences have a later onset,

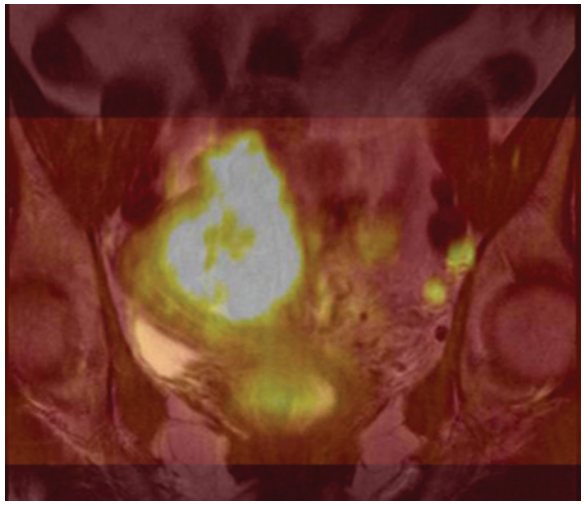

Figure 8. Advanced endometrial carcinoma in a 63-year-old woman. Fused image (false color map derived from a high *b*-value image [b = 800 sec/mm^2] superimposed on a coronal T2-weighted MR image) shows very high signal intensity in the tumor periphery, with central low signal intensity that represents necrosis. Despite the high signal intensity in the left obturator nodes, histologic analysis showed the nodes to be reactive only.

usually occurring after one to two cycles of chemotherapy. Radiation therapy may also initially cause increased ADC values due to hyperemia. Changes in ADC values following tumor embolization are often not seen until several days after treatment. Therefore, we have found that diffusion-weighted imaging and contrast-enhanced imaging are complementary in assessing response to therapy and should be interpreted with full knowledge of the patient's treatment schedule.

Potential Pitfalls in Image Interpretation

T2 Shine-through

It is important to remember that diffusion-weighted images are intrinsically T2 weighted and that tissues with slow T2 relaxation rates can appear bright. T2 shine-through refers to persistent hyperintensity seen on high *b*-value images with a corresponding high ADC value. The high ADC value will, therefore, also appear bright on ADC maps (Table 2). This phenomenon can cause problems in image interpretation when high *b*-value images are viewed in isolation without reference to corresponding ADC maps. This fact should be borne in mind when using the fusion software to superimpose high *b*-value images onto anatomic images (Fig 10). Figures 11 and 12 demonstrate two cases of vulval carcinoma.

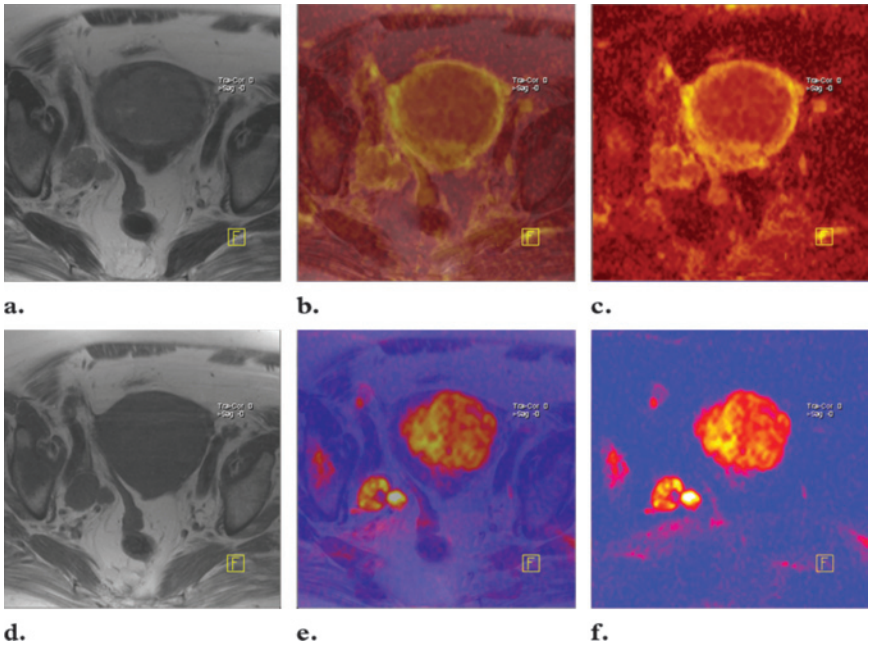

Figure 9. Advanced endometrial carcinoma in a 70-year-old woman with significant restriction to water diffusion. T2-weighted **(a)**, T2-weighted–ADC **(b)**, ADC **(c)**, T1-weighted **(d)**, T2-weighted–high *b*-value (b = 1000 sec/mm^2) **(e)**, and high *b*-value (b = 1000 sec/mm^2) **(f)** images show an endometrial carcinoma and enlarged right obturator lymph nodes, which also demonstrate marked restriction and have a signal intensity similar to that of the tumor.

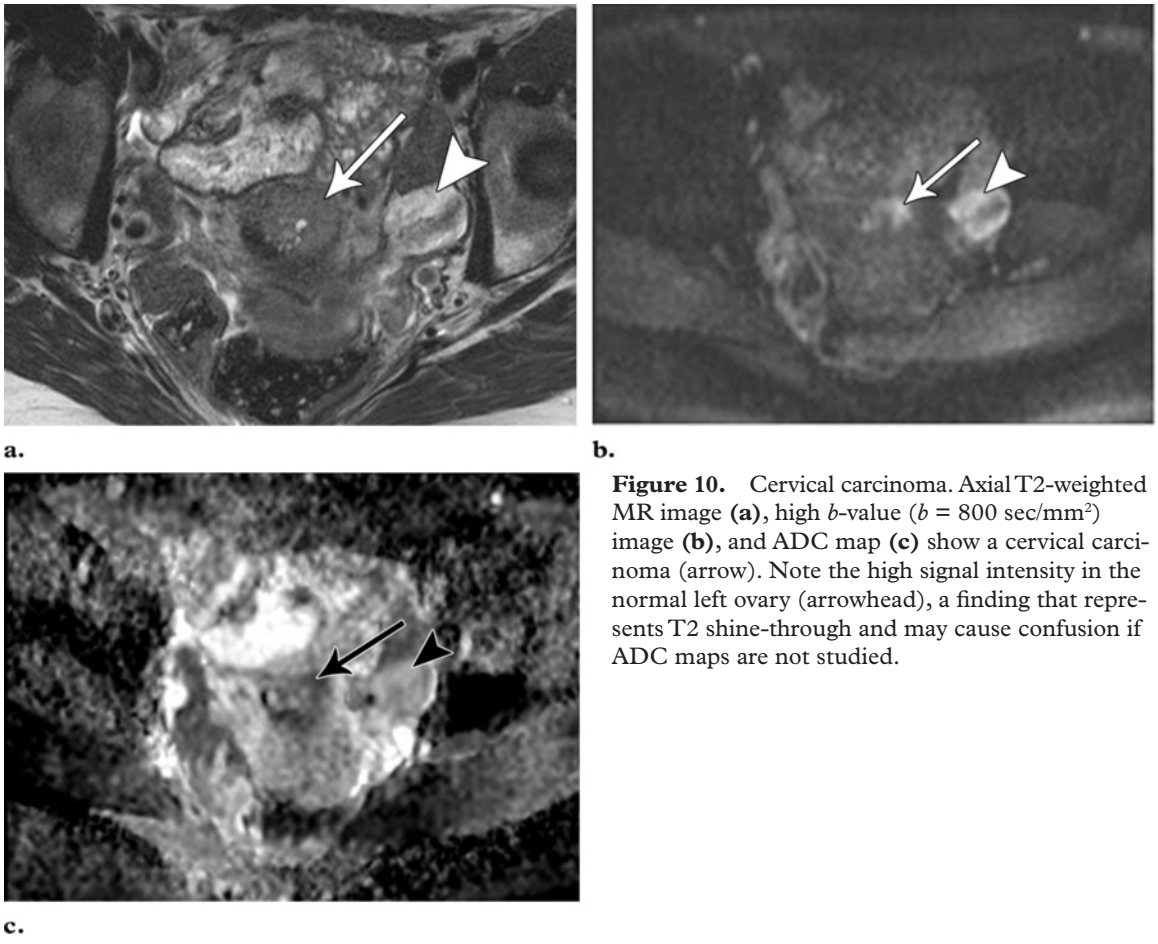

Figure 10. Cervical carcinoma. Axial T2-weighted MR image **(a)**, high *b*-value (b = 800 sec/mm^2) image **(b)**, and ADC map **(c)** show a cervical carcinoma (arrow). Note the high signal intensity in the normal left ovary (arrowhead), a finding that represents T2 shine-through and may cause confusion if ADC maps are not studied.

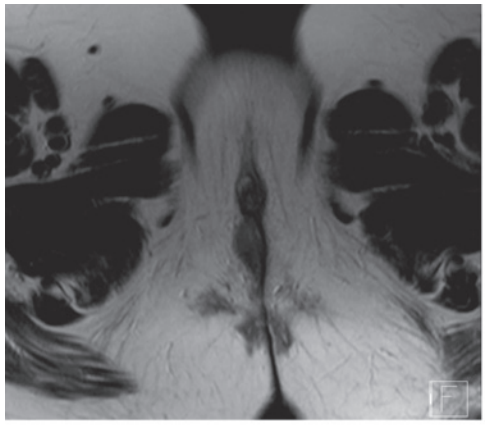

11a.

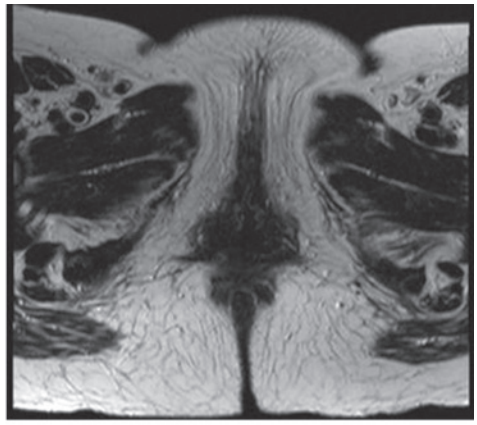

12a.

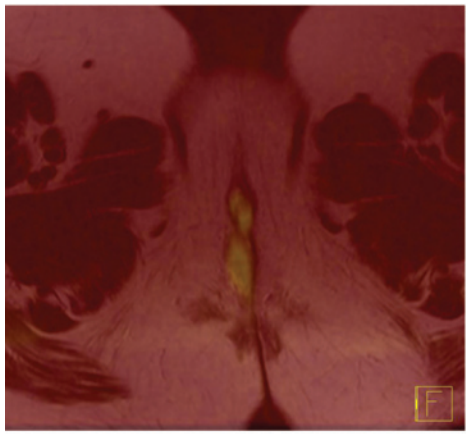

11b.

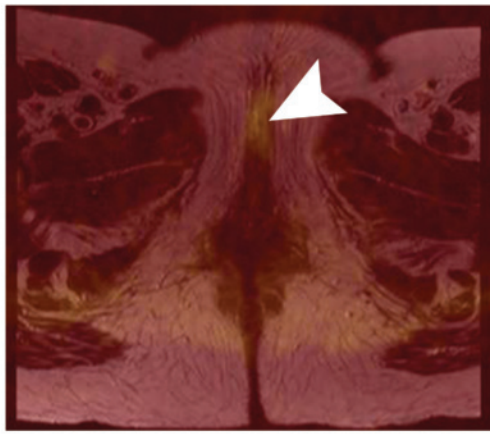

12b.

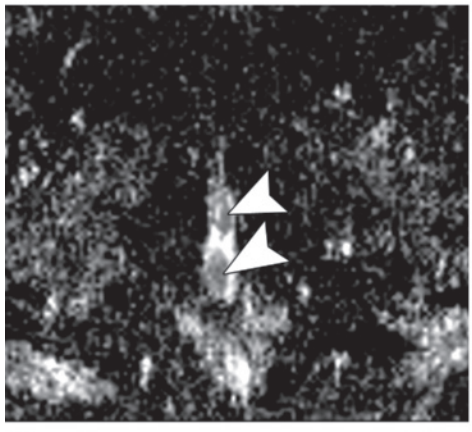

11c.

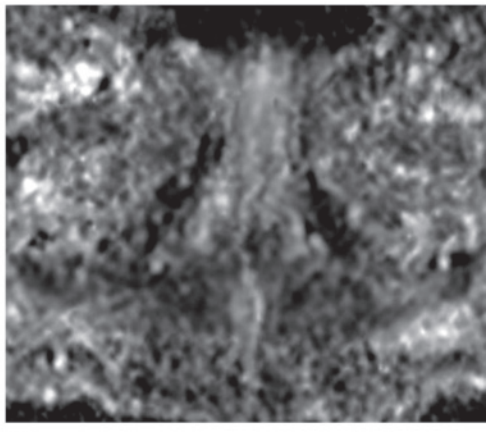

12c.

Figures 11, 12. **(11)** Vulval carcinoma in an 82-year-old woman. **(a)** On an axial T2-weighted MR image, the tumor is difficult to visualize. **(b)** Fused image (false color map derived from a high *b*-value image [b = 800 sec/mm^2] superimposed on **a**) clearly depicts the tumor. **(c)** Axial ADC map shows the tumor with low ADC values (arrowheads). **(12)** Vulval carcinoma in a 75-year-old woman in whom the primary tumor had been fully excised. Axial T2-weighted MR image **(a)**, fused image (false color map derived from a high *b*-value image [b = 800 sec/mm^2] superimposed on **a**) **(b)**, and ADC map **(c)** show a lesion. The high-signal-intensity area in **b** (arrowhead) represents postexcision edema, with no corresponding low-signal-intensity area on the ADC map. These findings contrast with those in Figure 11 and demonstrate the importance of viewing the entire examination.

a.

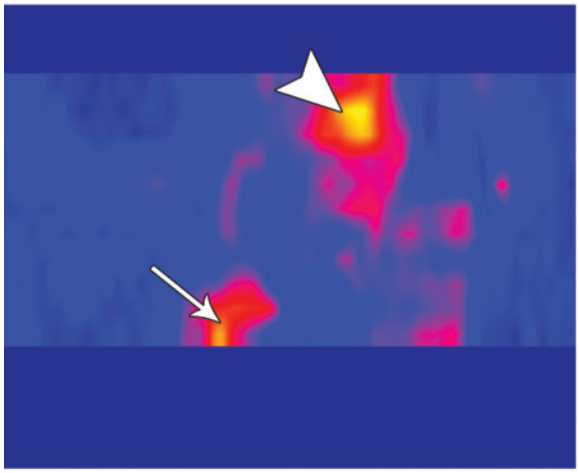

b.

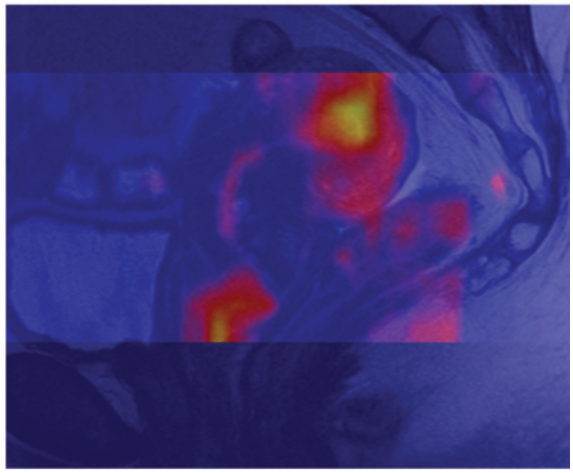

c.

Figure 13. Cervical carcinoma in a 39-year-old woman. **(a)** Sagittal T2-weighted MR image shows a large tumor on the anterior lip of the cervix. **(b)** False color map derived from a high *b*-value image (b = 800 sec/mm^2) shows high signal intensity in the tumor (arrow) and in the endometrium at the uterine fundus (arrowhead). **(c)** Fused image (**b** superimposed on **a**) helps confirm the location of the cervical tumor and the area of restriction in the fundal endometrium. No abnormality was seen in the uterine fundus at hysterectomy; thus, the endometrial findings are taken to represent restriction within the normal endometrium.

In Figure 11, the tumor is difficult to visualize on the T2-weighted image (Fig 11a) but is readily identified on the high *b*-value (b = 800 sec/mm^2) image (Fig 11b) and has a correspondingly low ADC value (Fig 11c). The appearance of the lesion in Figure 12b is very similar to that in Figure 11b, and the presence of residual tumor may be suspected. However, the high-signal-intensity area in Figure 12b has a high ADC value that reflects posttreatment edema.

Restriction in Normal Structures

Because diffusion-weighted MR imaging demonstrates areas of restriction to water diffusion, any areas of high cellular density will have high signal intensity on high *b*-value images. Normal endometrium in women of reproductive age is composed of endometrial glands and of stromal cells with high cellular density and abundant cytoplasm. In a study comparing endometrial cancers with normal endometrium, Tamai et al (4) found normal endometrium to have high signal intensity on high *b*-value (b = 1000 sec/mm^2) images. However, quantitative discrimination between normal endometrium and cancer was possible due to the significantly lower ADC value of tumor; thus, the hyperintensity of endometrium on high *b*-value images is due to T2 shine-through. Figure 13 shows a cervical cancer with a separate focal area of hyperintensity in the endometrium, which proved to be normal at subsequent hysterectomy.

Other normal structures with high cellular density that are also hyperintense on high *b*-value images include normal or reactive lymph nodes and bowel mucosa. Node assessments were discussed earlier. The fact that bowel mucosa can appear bright on high *b*-value images

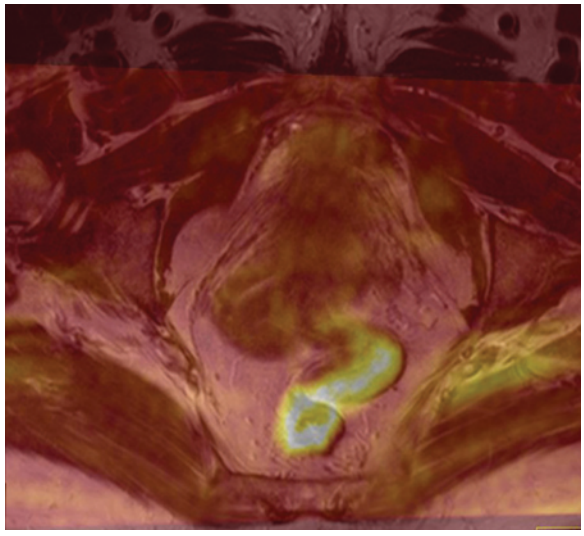

Figure 14. Endometrial carcinoma in a 69-year-old woman. Fused image (false color map derived from a high *b*-value image [b = 800 sec/mm^2] superimposed on an axial T2-weighted MR image from a staging examination) shows high signal intensity within the mucosa of the normal sigmoid colon, a finding that represents restriction to water diffusion.

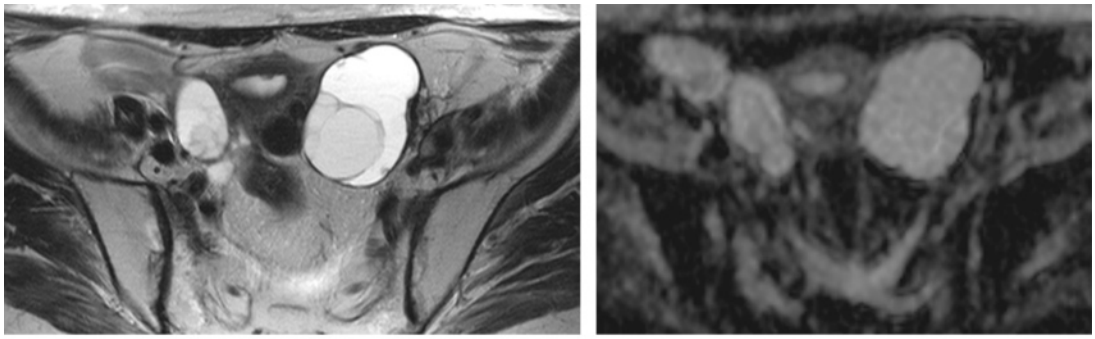

a. **b.**

Figure 15. Bilateral ovarian metastases from a well-differentiated endocervical adenocarcinoma. **(a)** Axial T2-weighted MR image shows bilateral complex adnexal cysts with predominantly high signal intensity. **(b)** ADC map shows the lesions with high ADC values, a finding that reflects free water diffusion due to the cystic nature of the lesions.

(Fig 14) may potentially confound the detection of microscopic peritoneal disease at high *b*-value diffusion-weighted MR imaging. For this application, diffusion-weighted imaging is most reliable around the paracolic reflections and omentum and in subdiaphragmatic areas.

Tumors with Low Cellular Density

Although diffusion-weighted MR imaging has been shown to be helpful in distinguishing normal tissue or benign lesions from malignant tumors (2,4–7), the success of the technique depends on the demonstration of restriction to water diffusion due to increased cellular density.

Teaching Point

In malignant tumors with low cellularity (eg, well-differentiated adenocarcinomas or ovarian cancers with large cystic components), restriction to water diffusion is likely to be much more limited and may not be visible at diffusion-weighted MR imaging (Fig 15).

Other Causes of Hyperintensity on High *b*-Value Images with Corresponding Low ADC Values

The combination of hyperintensity on source high *b*-value images and corresponding low ADC values is typically thought to be due to high cellular density in tumor tissue (with exceptions in normal tissue as described earlier). However, similar appearances can be seen in abscesses, areas of coag-

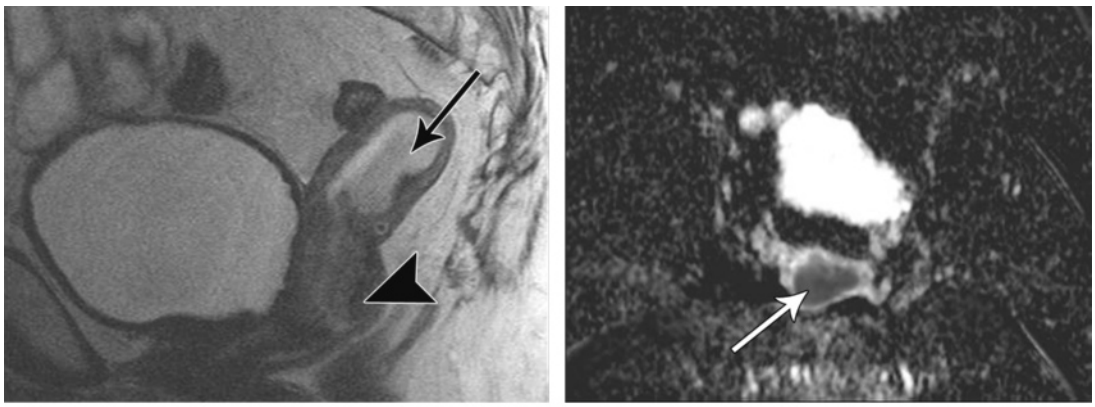

a. b.

Figure 16. Retained inspissated mucus within the endometrial cavity due to an obstructing cervical carcinoma. **(a)** Sagittal T2-weighted MR image shows a cervical tumor (arrowhead) with distention of the endometrial cavity by high-signal-intensity mucus (arrow). **(b)** ADC map shows the mucus (arrow) with a low ADC value, a finding that is likely due to the restriction of water molecules caused by the presence of macromolecules. In such cases, anatomic images are helpful in excluding the presence of tumor within the endometrial cavity.

ulative necrosis, and inspissated mucus (20–22). In coagulative necrosis, this finding is thought to be due to the retention of cellular outlines and architecture. In abscess and inspissated mucus, water restriction may be due to the presence of a large number of macromolecules. We have noted these appearances in patients with hydrosalpinx, in some ovarian cysts, and, occasionally, within an obstructed endometrial cavity (Fig 16).

Conclusions

High-quality diffusion-weighted MR imaging of the entire pelvis can now be performed as part of a gynecologic examination without greatly increasing total imaging time. Diffusion-weighted MR imaging provides important new information noninvasively. This unique modality is helpful in initial staging of known malignancies, differentiating benign from malignant lesions, assessing treatment response, and determining the presence of disease recurrence. To ensure accuracy, it is important to be aware of the potential pitfalls of diffusion-weighted MR imaging and to review findings in conjunction with findings obtained with anatomic sequences. Increasing familiarity with ADC calculation and manipulation software, including the ability to fuse anatomic and diffusion data, will allow radiologists to gain confidence and thus to provide new information to physicians who are caring for women with known or suspected gynecologic malignancies.

References

1. Koh DM, Collins DJ. Diffusion-weighted MRI in the body: applications and challenges in oncology. AJR Am J Roentgenol 2007;188:1622–1635.
2. Naganawa S, Sato C, Kumada H, Ishigaki T, Miura S, Takizawa O. Apparent diffusion coefficient in cervical cancer of the uterus: comparison with the normal uterine cervix. Eur Radiol 2005;15:71–78.
3. McVeigh PZ, Syed AM, Milosevic M, Fyles A, Haider MA. Diffusion-weighted MRI in cervical cancer. Eur Radiol 2008;18:1058–1064.
4. Tamai K, Koyama T, Saga T, et al. Diffusion-weighted MR imaging of uterine endometrial cancer. J Magn Reson Imaging 2007;26:682–687.
5. Inada Y, Matsuki M, Nakai G, et al. Body diffusion-weighted MR imaging of uterine endometrial cancer: is it helpful in the detection of cancer in nonenhanced MR imaging? Eur J Radiol 2008 Jan 5 [Epub ahead of print].
6. Tamai K, Koyama T, Saga T, et al. The utility of diffusion-weighted MR imaging for differentiating uterine sarcomas from benign leiomyomas. Eur Radiol 2008;18:723–730.
7. Fujii S, Matsusue E, Kigawa J, et al. Diagnostic accuracy of the apparent diffusion coefficient in differentiating benign from malignant uterine endometrial cavity lesions: initial results. Eur Radiol 2008;18:384–389.
8. Fujii S, Matsuse E, Kanasaki Y, et al. Detection of peritoneal dissemination in gynaecological malignancy: evaluation by diffusion-weighted MR imaging. Eur Radiol 2008;18:18–23.
9. Stejskal EO, Tanner JE. Spin diffusion measurements: spin-echo in the presence of a time dependent field gradient. J Chem Phys 1965;42:288–292.

10. Patterson DM, Padhani AR, Collins DJ. Technology insight: water diffusion MRI—a potential new biomarker of response to cancer therapy. Nat Clin Pract Oncol 2008;5:220–233.
11. Koh DM, Takahara T, Imai Y, Collins DJ. Practical aspects of assessing tumors using clinical diffusion-weighted imaging in the body. Magn Reson Med Sci 2007;6:211–224.
12. Shen SH, Chiou YY, Wang JH, et al. Diffusion-weighted single-shot echo-planar imaging with parallel technique in assessment of endometrial cancer. AJR Am J Roentgenol 2008;190:481–488.
13. Tangjitgamol S, Manusirivithaya S, Jesadapatarakul S, Leelahakorn S, Thawaramara T. Lymph node size in uterine cancer: a revisit. Int J Gynecol Cancer 2006;16:1880–1884.
14. Sumi M, Ichikawa Y, Nakamura T. Diagnostic ability of apparent diffusion coefficients for lymphomas and carcinomas in the pharynx. Eur Radiol 2007;17:2631–2637.
15. Sumi M, Van Cauteren M, Nakamura T. MR microimaging of benign and malignant nodes in the neck. AJR Am J Roentgenol 2006;186:749–757.
16. Hamstra DA, Rehemtulla A, Ross BD. Diffusion magnetic resonance imaging: a biomarker for treatment response in oncology. J Clin Oncol 2007;25:4104–4109.
17. Schepkin VD, Chenevert TL, Kuszpit K, et al. Sodium and proton diffusion MRI as biomarkers for early therapeutic response in subcutaneous tumors. Magn Reson Imaging 2006;24:273–278.
18. Chenevert TL, McKeever PE, Ross BD. Monitoring early response of experimental brain tumors to therapy using diffusion magnetic resonance imaging. Clin Cancer Res 1997;3:1457–1466.
19. Einarsdottir H, Karlsson M, Wejde J, Bauer HC. Diffusion-weighted MRI of soft tissue tumours. Eur Radiol 2004;14:959–963.
20. Noguchi K, Watanabe N, Nagayoshi T, et al. Role of diffusion-weighted echo-planar MRI in distinguishing between brain abscess and tumour: a preliminary report. Neuroradiology 1999;41:171–174.
21. Chang SC, Lai PH, Chen WL, et al. Diffusion-weighted MRI features of brain abscess and cystic or necrotic brain tumours: comparison with conventional MRI. Clin Imaging 2002;26:227–236.
22. Park SH, Chang KH, Song IC, Kim YJ, Kim SH, Han MH. Diffusion-weighted MRI in cystic or necrotic intracranial lesions. Neuroradiology 2000;42:716–721.

RadioGraphics

Diffusion-weighted MR Imaging of Female Pelvic Tumors: A Pictorial Review

Charlotte S. Wittaker, MRCP, FRCR et al

RadioGraphics 2009; 29:759–778 • **Published online** 10.1148/rg.293085130 • **Content Codes:** GU MR OB OI

Page 762
It is important to remember that ADC maps and high *b*-value images should never be interpreted in isolation, but should be interpreted together with anatomic images according to the scheme outlined in Table 2 so as to avoid the pitfalls that will be discussed shortly.

Page 762
Data sets can be visualized with use of multiplanar reconstruction and maximum intensity projection and are amenable to volume rendering. Such data are also amenable to fusion imaging to allow coregistration to anatomic images.

Page 767
High-grade adenocarcinomas typically have high cellular density and so would be expected to have lower ADC values.

Page 768
The success of therapy can be assessed both quantitatively with ADC measurements and qualitatively by inspecting signal intensity on high *b*-value images.

Page 772
In malignant tumors with low cellularity (eg, well-differentiated adenocarcinomas or ovarian cancers with large cystic components), restriction to water diffusion is likely to be much more limited and may not be visible at diffusion-weighted MR imaging (Fig 15).